

Topological solitons and bulk polarization switch in collinear type II multiferroics

D. C. Cabra

IFLySiB-CONICET and Departamento de Física, Universidad Nacional de La Plata, Argentina

A. O. Dobry and C. J. Gazza

*IFIR-CONICET and Facultad de Ciencias Exactas,
Ingeniería y Agrimensura, Universidad Nacional de Rosario, Argentina*

G. L. Rossini

IFLP-CONICET and Departamento de Física, Universidad Nacional de La Plata, Argentina

(ΩDated: March 18, 2024)

We introduce a microscopic model for collinear multiferroics capable to reproduce, as a consequence of magnetic frustration and easy-axis anisotropy, the so-called “uudd” (or antiphase) magnetic ordering observed in several type II multiferroic materials. The crucial role of lattice distortions in the multiferroic character of these materials is entered into the model via an indirect magnetoelectric coupling, mediated by elastic degrees of freedom through a pantograph mechanism. Long range dipolar interactions set electric dipoles in the antiferroelectric order. We investigate this model by means of extensive DMRG computations and complementary analytical methods. We show that a lattice dimerization induces an spontaneous \mathbb{Z}_2 ferrielectric bulk polarization, with a sharp switch off produced by a magnetic field above a critical value. The topological character of the magnetic excitations makes this mechanism robust.

PACS numbers: 75.85.+t, 75.10 Jm, 75.10 Pq

I. INTRODUCTION

Multiferroic materials, defined as those in which ferroelectricity and (anti)ferromagnetism coexist and interact, have become one of the most studied topics in the last few years, both from the experimental and the theoretical point of view. The possibility of magnetic writing via electric fields makes these materials a potential source of technological applications in data storage.

Among the most recent discoveries a type of magnetoelectric materials, so called type II multiferroics in which the electrical polarization coincides with a magnetic ordering transition, has been the subject of a lot of efforts [1,2]. What is most important in these materials is the very large coupling between magnetic and electrical properties, even if the value of the electrical polarization can be rather small as compared to typical ferroelectric materials.

An important issue is to determine the microscopic underlying general mechanism which could be applied to guide the synthesis of bulk or film materials with enhanced magnetoelectric properties (see *e.g.* [3] and references therein). Within the present paper we contribute to this task by proposing and analyzing a model in which this cross-coupling arises via the interaction with the lattice, thus fitting into the so called exchange-striction mechanism [1,2,4]

Very generally the high magnetoelectric response appears to be associated to the magnetic frustration due to competing spin interactions leading to complex magnetic orders [1]. Indeed, in most of multiferroic materials with collinear spins the magnetic order observed at low magnetic fields is of the “uudd” ($\uparrow\uparrow\downarrow\downarrow$) type along

some particular line (see for instance [1,2,5] and references therein). Such order usually appears when second neighbors antiferromagnetic interactions compete with either the uniform or Néel configurations induced by nearest neighbors interactions. This happens to be the case in quasi-one-dimensional materials like $\text{Ca}_3\text{CoMnO}_6$ [6], quasi-two-dimensional materials like the delafossite AgCrS_2 [7,8] and also in multiferroic manganite perovskites with E-type antiferromagnetic order such as HoMnO_3 [9,10], ferrite perovskites such as GdFeO_3 [11] and other 3D compounds such as the CdV_2O_4 spinel [12] or RNiO_3 nickelates ($\text{R}=\text{La, Pr, } \dots, \text{Lu}$) [13]. Among these $\uparrow\uparrow\downarrow\downarrow$ multiferroic materials, particular interest focuses on double perovskites such as $\text{Yb}_2\text{CoMnO}_6$ [14], $\text{Lu}_2\text{MnCoO}_6$ [15,16], $\text{Er}_2\text{CoMnO}_6$ [17], and R_2NiMnO_6 ($\text{R}=\text{Pr, Nd, Sm, Gd, Tb, Dy, Ho, and Er}$) where a giant magnetoelectric effect has been reported [18].

In a previous paper [19] we have introduced a simple microscopic multiferroic model describing a system with magnetic and electric dipolar degrees of freedom coupled via lattice distortions. This mediated coupling is ubiquitous in magnetoelectric phenomena and may be enhanced by the strong influence of the lattice in multilayer multiferroics, as in some cases the lattice mismatch of the layer and the substrate can generate enormous lattice distortions and trigger giant multiferroic responses [20,21].

In the present work we extend and generalize our previous study in several aspects: first and most important, we add antiferromagnetic exchange couplings between next nearest neighbors (NNN) reported in most of the above mentioned materials. When the NNN coupling is strong enough we reproduce the experimentally observed $\uparrow\uparrow\downarrow\downarrow$ magnetic ordering at zero magnetic field.

This confirms that magnetic frustration is at the root of the phenomenology observed in many materials. Second and in order to make closer contact with experiments, we introduce an easy axis anisotropy that mimics the effective Ising character observed for otherwise quantum magnetic moments. Indeed, the magnetic ions are immersed in crystal local fields that generally diminish their quantum character, making them behave as almost classical Ising variables. Good examples of this situation are the spin-ice pyrochlores [22], with the exception being Tb based pyrochlores where Ising models seem not to suffice but quantum fluctuations have to be included [23–25]. Thus a parameter controlling the easy axis anisotropy allows for a phase diagram covering the “quantum” and “classical” behavior realized in many possible different materials. Last but not least, we consider realistic dipolar interactions which either from intermediary itinerant electrons [26], from Coulomb forces [27], or by other effective mechanism, are expected to act as long range forces. Even when truncated at second neighbors, long range dipole-dipole interactions give rise to new phases in a richer dipole-elastic phase diagram.

Along this work we discuss the zero temperature ground state of the magnetic, electric and elastic one dimensional system described below. The main results will be the emergence of a spontaneous bulk polarization at zero magnetic field, as well as a sharp drop thereof once the magnetic field exceeds a critical value.

The paper is organized as follows: in Sect. II we define the microscopic model to be discussed, the regions of interest and the methods to be used. In Sect. III we explore the behavior of dipolar degrees of freedom in the absence of magnetism, finding that long range dipolar interactions give rise to a new intermediate phase with period three order. In Sect. IV we present our main results: the spontaneous electric polarization driven by the interactions and the switch off of this effect as soon as the system is magnetized by an external magnetic field. In Sect. V we summarize our results, discussing possible experimental tests and applications such as efficient polarization flip devices.

II. SYSTEM MODEL AND METHODS

A. The model

The system model under analysis describes magnetic, electric and elastic degrees of freedom, in which magnetic moments and electric dipoles interact independently with the lattice, that serves as the intermediary for the effective magnetoelastic coupling we want to describe.

Magnetoelastic sector. Magnetic ions positions are described as sites i in a linear chain. Their regular positions are $x_i = ia$ where a is a lattice constant but under distortions the ions move to $x_i + u_i$ along the chain direction, so that sites i and $i + 1$ will be separated by a

distance $a + \delta_i$ with $\delta_i = u_{i+1} - u_i$. The elastic energy cost of such distortions is given by

$$H_{\text{elastic}} = \frac{K}{2} \sum_i \delta_i^2, \quad (1)$$

where K is the lattice stiffness.

Magnetic ions themselves are represented by $S = 1/2$ spin operators \mathbf{S}_i at chain sites. While the model aims to describe the $\uparrow\uparrow\downarrow\downarrow$ order observed along certain lines in two and three dimensional multiferroic materials, it is interesting to notice that a few compounds that have been identified to become multiferroic do show this order in quasi-one-dimensional chains of Cu^{2+} magnetic ions ($S = 1/2$): for instance LiCuVO_4 [28,29], LiCu_2O_2 [30–32], CuCl_2 [33], CuBr_2 [34], $\text{PbCuSO}_4(\text{OH})_2$ [35,36], CuCrO_4 [37] and $\text{SrCuTe}_2\text{O}_6$ [38].

Following our proposal in [19], the magnetic ions interact via nearest neighbors (NN) antiferromagnetic couplings J_1 . Frustration is introduced by next nearest neighbors (NNN) antiferromagnetic couplings J_2 . Both NN and NNN super-exchange couplings have magnitudes that may depend on elastic distortions. However, we assume for simplicity that only the NN exchange shows a linear dependence that can be written as

$$J_1(\delta_i) = J_1(1 - \alpha\delta_i) \quad (2)$$

where $\alpha > 0$ is called the linear magnetoelastic coupling (incidentally, in the frequent case of alternating distortions the second neighbor distances $2a + \delta_i + \delta_{i+1}$ are not altered at all). Positive α makes NN exchange stronger as magnetic ions approach each other.

The effect of crystal fields can in general be modeled by anisotropic spin interactions: the $SU(2)$ invariant Heisenberg interaction $\mathbf{S}_i \cdot \mathbf{S}_j$ is replaced by $S_i^x S_j^x + S_i^y S_j^y + \Delta S_i^z S_j^z$ (z axis determined by the crystal environment). Aiming to describe collinear multiferroic materials, we focus on $\Delta \geq 1$; that is, we cover the easy axis anisotropy case $\Delta > 1$ and in particular the isotropic case $\Delta = 1$. This is motivated by the large variety of known multiferroic materials, but also by the theoretical importance of the $SU(2)$ invariant point case. The easy plane regime $\Delta < 1$, not discussed here, is known to be continuously connected with the isotropic case (see for instance [39]). On the other hand, the limit $\Delta \rightarrow \infty$ connects our work with the classical Ising regime. In order to deal with large Δ without hiding the other sectors, we introduce a parameter $\gamma \equiv 1/\Delta$ and absorb Δ into the exchange constants. Finally, we introduce the Zeeman energy associated with an external magnetic field h along the easy axis direction.

The magnetic sector, coupled to lattice distortions, is then described by the Hamiltonian

$$H_{\text{spin}} = \sum_i J_1(\delta_i) (\mathbf{S}_i \cdot \mathbf{S}_{i+1})_\gamma + \sum_i J_2 (\mathbf{S}_i \cdot \mathbf{S}_{i+2})_\gamma - h \sum_i S_i^z, \quad (3)$$

dipoles amidst magnetic ions, with a natural magnitude p_0 and a preferred axis $\hat{\mathbf{e}}$ oriented perpendicular to the chain (this choice of axes can be easily generalized to deal with more general situations, but the main novelty of the mechanism presented here is already contained in this simplified description). Under distortions δ_i the local dipole magnitude is modified through a pantograph mechanism [19,53,54]. This is modeled in a linear approximation by $\mathbf{p}_i = p_i(\sigma_i, \delta_i)\hat{\mathbf{e}}$ with a component

$$p_i(\sigma_i, \delta_i) = p_0 (1 - \beta \delta_i) 2\sigma_i. \quad (5)$$

Here $\sigma_i = \pm 1/2$ is an Ising variable for the orientation of the dipole along its axis, p_0 is the dipolar moment magnitude in the absence of distortions, and β will be called the dipole-elastic coupling. Notice that $\beta > 0$ makes dipolar moments larger as neighboring magnetic sites become closer. The pantograph mechanism, depicted in Fig. 2, encodes the interaction between electric dipoles and elastic degrees of freedom. Rombooids in this picture represent, without loss of generality, the actual crystal environment of magnetic ions.

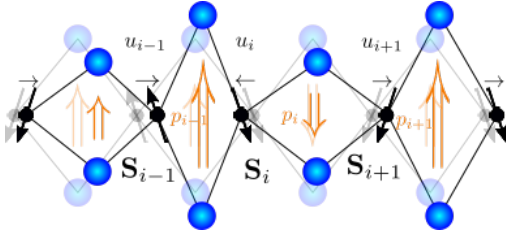


FIG. 2: Cartoon of degrees of freedom and dipole-elastic coupling mechanism. Magnetic ions are described as a chain of sites (in black) while dipoles (double arrows) associated to charged ions (in blue) are located at chain bonds. Displacements of magnetic ions u_i modify bond lengths by a distortion $\delta_i = u_{i+1} - u_i$. Also the distance between adjacent dipoles is distorted by $\eta_i = (\delta_i + \delta_{i+1})/2$. A dipole strength is enlarged (shortened) when the bond is shortened (enlarged) while its orientation is given by an Ising variable, as described in Eq. 5. Shaded symbols show the undistorted (regular) lattice, full colored symbols represent a general distortion configuration.

For a given distribution of distortions δ_i and dipoles $p_i(\sigma_i, \delta_i)$ the system acquires a bulk polarization

$$P \equiv \frac{1}{N_s} \sum_{i=1}^{N_s} p_i(\sigma_i, \delta_i) = \frac{1}{N_s} \sum_{i=1}^{N_s} p_0 (1 - \beta \delta_i) 2\sigma_i, \quad (6)$$

where N_s is the chain length (number of sites).

Electric dipolar momenta may interact with each other, at a relevant energy scale, in a phenomenological way. Such interaction is eventually determined by long range dipole-dipole interactions and/or elastic relations between deformations of charged and intermediate ions in the crystal [55]. For the sake of definiteness we consider a Coulomb long range dipole-dipole interaction coupling decaying with the cube of the dipole separation,

$$\lambda_D \frac{\mathbf{p}_i \cdot \mathbf{p}_j - 3(\mathbf{p}_i \cdot \hat{\mathbf{x}})(\mathbf{p}_j \cdot \hat{\mathbf{x}})}{|x_j - x_i|^3} \quad (7)$$

which in the present geometry only contributes with the product of the transverse components p_i . Regarding the distance decay, notice that dipoles p_i and p_{i+1} are separated by a distance $a + \eta_i$, where $\eta_i = (\delta_i + \delta_{i+1})/2$ is the distortion of the distance between adjacent dipoles. The electric energy of a given configuration of dipoles coupled to distortions is given by

$$\begin{aligned} H_{\text{dipole}}^{(\text{full range})} &= \lambda_D \sum_i \left(\frac{p_i(\sigma_i, \delta_i) p_{i+1}(\sigma_{i+1}, \delta_{i+1})}{(a + \eta_i)^3} \right. \\ &+ \frac{p_i(\sigma_i, \delta_i) p_{i+2}(\sigma_{i+2}, \delta_{i+2})}{(2a + \eta_i + \eta_{i+1})^3} + \dots \\ &- E \sum p_i(\sigma_i, \delta_i) \end{aligned} \quad (8)$$

where the dots represent longer range dipolar interactions and E is an external electric field along the dipolar axis $\hat{\mathbf{e}}$. An electric field component transverse to this axis would introduce dipolar quantum fluctuations, interesting in the context of molecular magnets [56] or the ferroelectric SrTiO_3 [57] but this is out of the scope of the present work.

We consider here an expansion of the dipolar interactions in Eq. (8) up to second neighbors. We expect that the inclusion of longer range terms will not modify qualitatively the arising dipolar phases, at least for bipartite lattices where further neighbors fall into either the first or the second neighbor sublattices and will only renormalize the frustration. Assuming small deformations we also expand distortions up to linear terms. We get

$$\begin{aligned} H_{\text{dipole}} &= J_e \sum_i \left(\sigma_i \sigma_{i+1} + \frac{1}{8} \sigma_i \sigma_{i+2} \right) - 2\epsilon \sum_i \sigma_i + 2\beta\epsilon \sum_i \delta_i \sigma_i \\ &- J_e \sum_i \left[\left(\beta + \frac{3}{2a} \right) (\sigma_{i-1} \sigma_i + \sigma_i \sigma_{i+1}) + \frac{1}{8} \left(\beta + \frac{3}{4a} \right) (\sigma_{i-2} \sigma_i + \sigma_i \sigma_{i+2}) + \frac{3}{16a} \sigma_{i-1} \sigma_{i+1} \right] \delta_i, \end{aligned} \quad (9)$$

where $J_e \equiv 4\lambda_D p_0^2 / a^3$ and $\epsilon \equiv 2p_0^2 E$. A model described

by the addition of $H_{\text{elastic}} + H_{\text{dipole}}$ might be called a

dipole-Peierls system.

Complete Hamiltonian. As we mentioned at the beginning of this Section, the elastic degrees of freedom with the Hamiltonian given in Eq. (1), coupled separately to the spins in Eq. (3) and to the dipoles in Eq. (9), are the intermediaries of the magnetoelastic coupling in our proposal. This is achieved by the complete Hamiltonian to be discussed below,

$$H = H_{\text{elastic}} + H_{\text{spin}} + H_{\text{dipole}}, \quad (10)$$

that will be called the spin-dipole-Peierls Hamiltonian.

$$\begin{aligned} K\delta_i^{\text{free}} = & \alpha J_1 \langle S_i^z S_{i+1}^z + \gamma (S_i^x S_{i+1}^x + S_i^y S_{i+1}^y) \rangle - \beta \varepsilon \sigma_i \\ & + J_e \left(\beta + \frac{3}{2a} \right) (\sigma_{i-1} \sigma_i + \sigma_i \sigma_{i+1}) + \frac{1}{8} J_e \left(\beta + \frac{3}{4a} \right) (\sigma_{i-2} \sigma_i + \sigma_i \sigma_{i+2}) + J_e \frac{3}{16a} \sigma_{i-1} \sigma_{i+1}, \end{aligned} \quad (11)$$

further constrained by the fixed chain length condition $\delta_i = \delta_i^{\text{free}} - \bar{\delta}_i^{\text{free}}$ where the bar stands for average value along the chain.

On the one hand these self-consistent (SC) equations clearly exhibit the interplay between magnetic and electric degrees of freedom either collaborating or competing to produce the optimal elastic distortions. Each of them enters in the form of local correlations. On the other hand it allows to incorporate the knowledge about the magnetic sector and the electric sector separately. It should be stressed that NNN magnetic interactions, although not explicit in Eq. (11), play a central role in the actual value of NN correlations by introducing magnetic frustration in the Hamiltonian in Eq. (3). It is the analysis of this Hamiltonian what allows for theoretical or numerical input into the SC equations. Below we both discuss theoretical arguments and provide numerical results by iteratively solving the spin problem with the help of Density Matrix Renormalization Group (DMRG) computations [59].

We have performed an iterative numerical analysis based on DMRG to solve the magnetic and electric sectors in the adiabatic equations (6), along the lines stated in [58] and implemented in a similar context in [19]. The ground state for the spin system is obtained by the DMRG algorithm for each δ_i and σ_i configuration. Therefore, we re-obtain the set of δ_i from Eq. (11) and prove different σ_i in order to minimize the total energy. We have used periodic boundary conditions, and we have kept the truncation error less than $O(10^{-12})$, during up to more than 100 sweeps in the worst cases. This assures that errors of the DMRG computation are smaller than symbol sizes in each figure.

B. Self-consistent equations

In order to cope with the three coupled degrees of freedom, one needs an organizing strategy. Here we follow a self-consistent method [58] looking for the elastic distortions that minimize the total energy in Eq. (10).

For a given configuration of dipoles σ_i and a (quantum or classical) state for the spins \mathbf{S}_i , the minimal elastic energy is obtained when distortions δ_i satisfy the local zero gradient conditions

C. Regions of interest

The various parameters in the model allow for a rich phase diagram. According to the multiferroic materials we aim to describe, the main region of interest along the present work will be that with large enough ratio J_2/J_1 so as to manifest magnetic frustration. For large anisotropy $\gamma \ll 1$ one could expect that spin fluctuations are strongly diminished, allowing for a “uudd” ground state comparable to the classical ANNNI model antiphase state. However, we will show that quantum fluctuations still influence the deep Ising limit.

As for the energy scales, the dipolar exchange J_e will be kept below the magnetic exchange couplings, so that in principle it is magnetism what drives electric responses. The lattice stiffness K will set an energy scale larger than magnetic and electric ones, in order to keep distortions small with respect to the lattice spacing a . We set the length scale by taking the lattice spacing $a = 1$ and also set the energy scale taking $Ka^2 = 1$.

From the above considerations, we choose for numerical computations a reference set of phenomenological parameters $J_1 = 0.5$, $J_2 = 0.4$ and $J_e = 0.2$ to organize the energy scale of each degree of freedom. We also choose $\alpha = \beta = 0.2$ to analyze the magnetoelastic and electroelastic couplings. Notice that our results do not depend on fine tuning, so we expect them to be valid in a wide region of parameters.

The electric and magnetic fields in Eqs. (3, 8) can be varied in order to set the system in different polarized and magnetized regimes. Finally, the magnetic anisotropy will be varied from the quantum SU(2) symmetric point $\gamma = 1$ down to small enough values to explore the large easy axis anisotropy regime where classical behavior is expected.

III. POLARIZATION PROCESS IN THE PRESENCE OF AN ELECTRIC FIELD

In this Section we discuss the polarization due to an external electric field, when the magnetic sector is decoupled from the classical degrees of freedom ($\alpha = 0$). To this end we analyze the minimum energy configurations of the dipole-Peierls Hamiltonian $H_{\text{dipole}} + H_{\text{elastic}}$: given different periodic dipolar patterns we analytically compute the distortions minimizing the elastic energy, in the presence of the electric field. By comparison we select the lowest energy electroelastic configuration. In detail, we have considered all of the ordered dipolar configurations up to period four. The results lead to the dipole-elastic phase diagram in Fig. 3.

It should be stressed that long range dipole-dipole interaction leads to a richer phase diagram, with respect to the first neighbors interaction case [19]. It includes a new exotic phase where dipoles order with a period of three sites, not found before. Distortions occur with the same periodicity and will eventually contribute or interfere with the well-known period three magnetic plateau state that is expected for the magnetoelastic sector [60]. In the present one-dimensional case, and in any bipartite lattice, we expect no other qualitative changes by including the interactions between further neighbors.

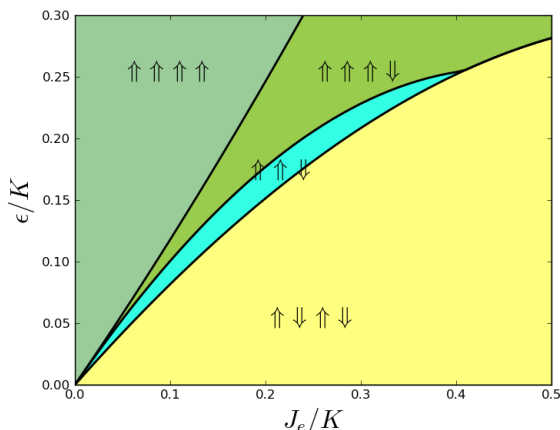


FIG. 3: Dipole-elastic phase diagram, computed for $\beta = 0.2$. Double line arrows describe the dipole ordered pattern in each region. Elastic distortions follow the dipole pattern periodicity, except in the zero field line $\epsilon = 0$ and the saturation region $\uparrow\uparrow\uparrow\uparrow$ where magnetic ions are equally spaced.

Without electric field the system possesses a \mathbb{Z}_2 inversion symmetry, but spontaneously adopts one of the two possible antiferroelectric $\uparrow\downarrow\uparrow\downarrow$ configurations. To be precise, these are described by

$$\sigma_i = (-1)^{i+\nu}, \quad (12)$$

where $\nu = 0$ (1) indicates whether odd (even) dipoles are pointing in the positive preferred axis direction. The distortions are null in either configuration, then dipoles

pointing up or down have the same magnitude and the system has no net polarization. This is shown with shaded circles in Fig. 4, with the left-most dipole pointing upwards; the other possibility is got by inversion, or equivalently by a one-site translation.

When a small electric field is turned on, breaking the inversion symmetry, no dipole flips are produced below a critical field but dimerized distortions are induced

$$\delta_i = -(-1)^{i+\nu} \frac{p_0 \beta}{K} \epsilon, \quad (13)$$

Under these distortions bonds with dipoles pointing along the field get shorter, enlarging the corresponding local dipolar momenta while bonds with dipoles pointing counter field get longer, shortening the corresponding dipolar strength. This behaviour is sketched in Fig. 4, and occurs in either antiferroelectric configuration ($\nu = 0, 1$). The bulk polarization reads

$$P(\epsilon) = \frac{1}{N_s} \sum_{i=1}^{N_s} p_0 (1 - \beta \delta_i) 2\sigma_i = \frac{p_0^2 \beta^2}{K} \epsilon. \quad (14)$$

That is, the system behaves as a simple paraelectric, acquiring a bulk polarization proportional to the applied electric field (with electric susceptibility $\chi_e = \frac{\partial P}{\partial E} = \frac{2p_0^4 \beta^2}{K}$).

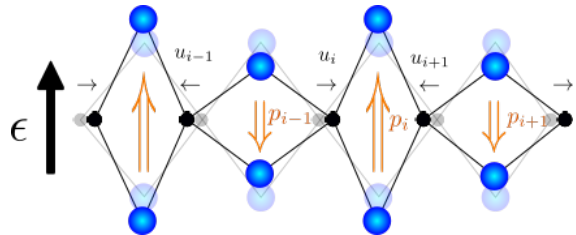


FIG. 4: Dipolar pattern in the dimerized electroelastic phase $\uparrow\downarrow\uparrow\downarrow$, for a finite electric field pointing upwards (symbols as in Fig. 2). Dipoles pointing along the field are larger than dipoles in the opposite direction. The alternation of bond length distortions is the mechanism for bulk polarization. The system acquires a linear electrical polarization (paraelectric behaviour). Distortions are magnified for visual effect.

At the critical line that separates the antiferroelectric low field phase from longer period dipolar structures, polarization gets discontinuous because of extensive dipolar flips. In the present work we concentrate in the low field region properties. Discontinuous transitions to higher polarized states, either via an electric or a magnetic field and the interplay with magnetization plateaus discussed below will be studied elsewhere.

IV. MAGNETO-ELASTIC COUPLING AND SPONTANEOUS ELECTRIC POLARIZATION

When the magnetic sector is coupled to the lattice through $\alpha \neq 0$, the ground state magnetic configuration may come along with lattice distortions. These in

turn bring about the possibility of modulations in the exchange couplings, associated to the lattice distortions.

In the absence of dipolar degrees of freedom this interplay between distortions and modulated exchange couplings is resolved as an energy balance between elastic cost and magnetic energy gain. Technically, this balance is expressed by self consistent equations similar to our Eqs. (11). In general, when non trivial distortions show up in the ground state, the spin excitation spectrum is gapped. In consequence the magnetization curve presents a plateau: it requires a finite magnetic field for the Zeeman energy to overcome the energy gap and change the spin state. A most important example is the spin-Peierls mechanism that promotes the formation of spin singlets at the cost of dimerized distortions [61,62], either in the non-frustrated case $J_2 = 0$ or the frustrated one [58]. This has been studied not only in one dimensional spin chains but also in higher dimensions [63–67]. The spin-lattice coupling also provides mechanisms for the opening of plateaus at different magnetization fractions, either for quantum $S = 1/2$ spins [68] or classical spins [69].

It is important to notice that magnetization plateaus may be related to other mechanisms, different from elastic distortions. One of them is the competition between NN and NNN exchange couplings, frustrating the antiferromagnetic order [44,70]. Moreover, the easy axis anisotropy drives a competition between the convenience of ground states with quantum structures (singlets) or classical frustrated configurations [71].

In our system model the magnetic frustration and the magnetoelastic mechanism co-exist, along with a dipolar energy cost/gain for lattice distortions. Altogether, this is expressed in the self consistent Eqs. (11) for lattice distortions. These SC equations show that the pantograph mechanism puts dipolar and magnetic correlations in either cooperation or competition with each other to produce changes in the bond lengths. *This is the key ingredient that provides an effective magnetoelectric coupling mediated by lattice distortions*, opening an avenue to a plethora of new physics.

We show below that this interplay gives rise to a bulk polarization without the presence of an external electric field. Moreover, we show that a magnetic field above a threshold causes a sharp polarization switch.

To start our analysis we first address to the existence of a zero magnetization plateau in the magnetization curve of the present spin-dipole-Peierls model, at zero electric field. As discussed in Section II C, we focus on the region with high enough frustration so as to produce the $\uparrow\uparrow\downarrow\downarrow$ magnetic ordering (see Fig. 1); for numerical work we take as a representative case the parameters $J_1 = 0.5$, $J_2 = 0.4$, $J_e = 0.2$, $\alpha = \beta = 0.2$. We have explored the anisotropy range $\gamma \leq 1$ and found signals of quantum and classical behaviour; we report, as representative examples, the $SU(2)$ symmetric case $\gamma = 1$ and a highly anisotropic case $\gamma = 1/8$.

We solved the self-consistent equations (11) iteratively, feeding in the spin-spin correlations computed by DMRG

in the presence of distortions and the zero electric field antiferroelectric dipolar configuration (see Fig. 3).

By covering all the possible magnetizations in a finite size chain of length N_s we draw the magnetization curves shown in Fig. 5 where the magnetization M is defined as the total $\langle S_{\text{total}}^z \rangle$ relative to saturation.

The outcome is a very rich phase diagram that not only includes previously studied situations, but also suggests some exotic non-trivial ones. Besides the $M = 0$ plateau present for both the isotropic and the anisotropic case, one can see other plateaus at simple fractions of the saturation magnetization. In particular, there is a noticeable plateau at $M = 1/3$ that is much wider in the anisotropic case, and comes together with a period three distortion modulation. There are also plateaus at $M = 1/2$ and $M = 2/3$ in the isotropic case, which are no longer present in the anisotropic case. In spite of small differences or special points, it is interesting to notice that the bosonization picture, strictly valid for $|\gamma| \geq 1$ ($|\Delta| \leq 1$), remains essentially the same for the easy axis anisotropic region $\gamma < 1$.

For completeness, we have computed the magnetization curves for systems with some lower frustration values ($J_2/J_1 = 0.2, 0.5$). We sketch in Fig. 6 a summary of the observed plateaus in a plane h vs. J_2/J_1 .

We will focus on the zero magnetization plateau and its magnetic excitations in the present work, with emphasis on the description of experimental setups attainable in the multiferroic materials surveyed in the Introduction. Finite magnetization plateaus, which could trigger further experiments in high magnetic fields, will be studied elsewhere.

A. Zero magnetization plateau

In this Section we compare the magnetic structure of the $M = 0$ plateau state observed in the $SU(2)$ isotropic case ($\gamma = 1$) and the easy axis anisotropic case ($\gamma = 1/8$). In spite of their differences, we will show that both of them lead to alternating distortions and produce a finite bulk polarization at zero electric field. Moreover, quantum fluctuations are relevant, though substantially damped, even for the (Ising-like) large anisotropic limit.

1. Quantum dimerized plateau

It is well known that, without exchange modulation ($\alpha = 0$) and with $\gamma = 1$, the homogeneous isotropic frustrated spin $S = 1/2$ antiferromagnetic Heisenberg chain spontaneously breaks the translation symmetry and enters a quantum dimer phase for $J_2/J_1 > 0.2411$ [39,45,46], with $\langle S_i^z \rangle = 0$ and spin correlations dominated by strong antiferromagnetic (negative) correlations every two-bonds (strictly, this is not collinear). The possibility of forming dimers in even or odd bonds makes the ground state two-fold degenerate.

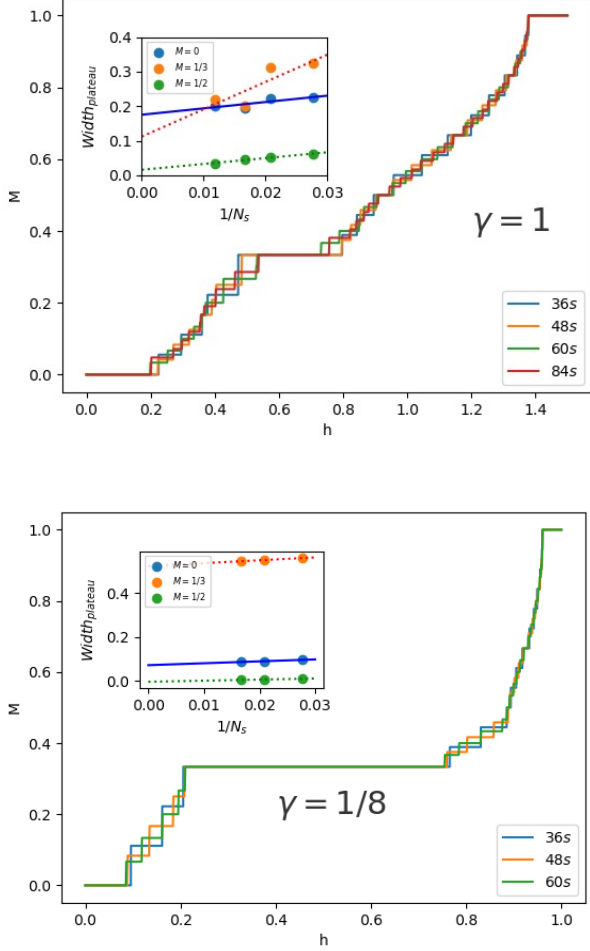


FIG. 5: Magnetization curves obtained by DMRG self-consistent solution of Eqs. (11) for the isotropic case ($\gamma = 1$) and a high easy axis anisotropy ($\gamma = 1/8$), setting $J_1 = 0.5$, $J_2 = 0.4$, $J_e = 0.2$, $\alpha = \beta = 0.2$ and zero electric field. A plateau at $M = 0$ is observed in both cases, though the spin structure found for isotropic case (quantum dimerized plateau) is very different from the one found in the anisotropic case (classical $\uparrow\uparrow\downarrow\downarrow$ plateau), see discussion below. A prominent plateau at magnetization fraction $M = 1/3$ is also observed in both cases. The insets show the finite size scaling of the main plateaus width.

In the presence of the magnetoelastic coupling in Eq. (2) the NN spin-spin correlations have influence on elastic distortions, as seen in the first line of Eqs. (11). As the frustrated spin-spin correlations alternate along the chain, frustration favors alternating distortions with short bonds accompanying spin singlets. Regarding the electroelastic coupling, one can see that the antiferroelectric configuration at zero electric field has site independent dipole-dipole correlations (negative between first neighbors, positive between second neighbors). According to the second line in Eqs. (11), and taking into account the fixed length constraint, dipole-dipole corre-

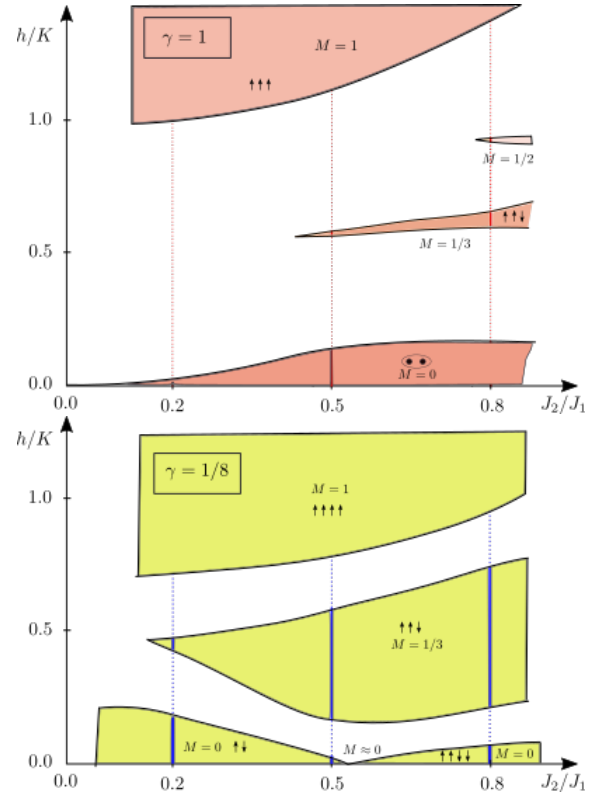


FIG. 6: Schematic magnetic phases showing the appearance of plateaus from the competition between the frustrated exchange J_2/J_1 and the magnetic field h , as well as the spin-lattice coupling. We report separately the isotropic case (top panel, $\gamma = 1$) and a highly anisotropic case (bottom panel, $\gamma = 1/8$). M is the magnetization relative to saturation, arrows indicate classical collinear order and points in an ellipse indicate quantum singlet dimers. We do not intend to depict here the $J_2/J_1 \rightarrow 0$ limit. The vertical lines correspond to magnetization curves at $J_2/J_1 = 0.2, 0.5$ and 0.8 , where solid segments indicate plateau ranges ($J_1 = 0.5$, $J_e = 0.2$, $\alpha = \beta = 0.2$).

lations have no influence on distortions. Thus, our model gets alternating distortions following the frustrated spin correlations. The strength of the dipoles sitting in shortened bonds is enlarged, while that of dipoles sitting in enlarged bonds is shortened (see Eq. (5)). As a consequence the magnetic frustration gives rise to a *ferrielectric* state, carrying a spontaneous bulk electric polarization. Such a bulk polarization, due to incomplete compensation of local dipole moments, has been observed in several multiferroic materials; besides the AgCrS_2 [8] that motivates our system model, well studied materials like TbMnO_3 and TbMn_2O_5 [72,73] are clear examples.

Notice that the two-fold degeneracy of the magnetic sector makes it possible to locate spin singlets (short bonds) either where dipoles point up or down. The spontaneous polarization then has two possible orientations, as dictated by the \mathbb{Z}_2 inversion symmetry of the model.

The present analysis for the frustrated isotropic mag-

netoelastic chain reinforces our previous results in the absence of frustration [19] where spontaneous polarization was only due to the spin-Peierls instability of nearest neighbors Heisenberg spin chains.

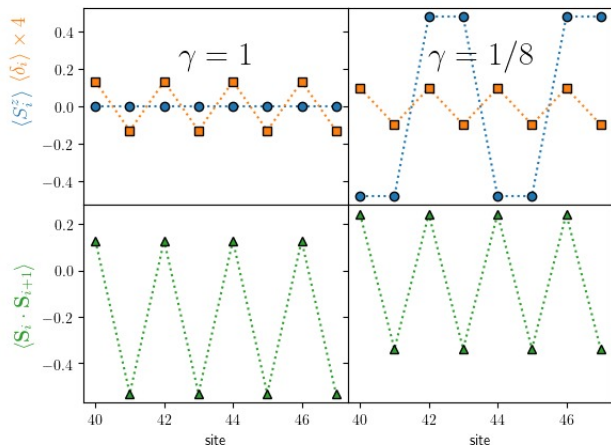


FIG. 7: Zoomed view of the $M = 0$ plateau configuration in a chain of 84 sites with periodic boundary conditions ($J_1 = 0.5$, $J_2 = 0.4$, $J_e = 0.2$, $\alpha = \beta = 0.2$, in the presence of an antiferroelectric dipolar background). Upper panels: local profile of $\langle S_i^z \rangle$ (blue circles) and distortions δ_i (orange squares), in the isotropic case (left panels, $\gamma = 1$) and highly anisotropic case (right panels, $\gamma = 1/8$). Distortions are scaled by a convenient factor for better visualization. Lower panels: local profile of spin correlations $\langle \mathbf{S}_i \cdot \mathbf{S}_{i+1} \rangle$ in the isotropic and anisotropic cases. In the isotropic case the vanishing of $\langle S_i^z \rangle$ and the enhanced alternated antiferromagnetic correlations are signals of a quantum dimer phase. In the anisotropic case the consecutive $\langle S_i^z \rangle \approx \pm 0.5$ and the alternation of ferromagnetic and antiferromagnetic correlations $\langle \mathbf{S}_i \cdot \mathbf{S}_{i+1} \rangle \approx \pm 0.25$ indicate a classical $\uparrow\uparrow\downarrow\downarrow$ phase. In both cases distortions are negative (short bonds) when spin correlations are negative (antiferromagnetic).

For concreteness, we show in the left panels of Fig. 7 the local spin expectation value, the distortion profile and spin-spin correlations obtained by solving Eqs. (11) for $J_1 = 0.5$, $J_2 = 0.4$, $J_e = 0.2$, $\alpha = \beta = 0.2$, $\gamma = 1$. As anticipated, there are alternating lattice distortions. The local magnetization vanishes, $\langle S_i^z \rangle = 0$. The spin-spin correlations are strongly antiferromagnetic where the bonds are shortened, and weakly ferromagnetic along enlarged bonds; this indicates the formation of spin singlets every two bonds and defines the quantum dimer phase. A second degenerate solution looks the same, but with dimers translated by one lattice site. A pictorial description of this states, including enlarged dipolar moments at singlet bonds, is shown in Fig. 8.

In the presence of an electric field (not enough to produce dipole flips, see Fig. 3), the dipole-field term in the SC equations also favors the alternation of distortions. But now it selects the short bonds to be located where dipoles point along the field (as already discussed in the

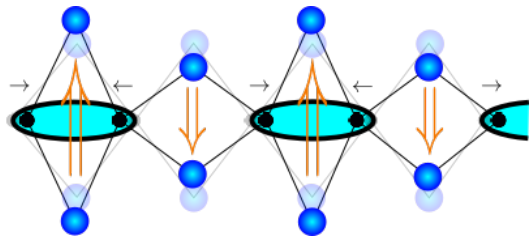


FIG. 8: Schematic picture for the quantum plateau state at $M = 0$. The two-spin singlets represented by ellipses gain magnetic energy by shortening their distance, thus enlarging their exchange coupling. The influence of these distortions on the alternating dipoles lengths (double arrows) produces a ferrielectric configuration with a finite bulk polarization.

electroelastic sector, see Section III). In other words, an infinitesimal poling electric field breaking the \mathbb{Z}_2 symmetry is enough to select one of the otherwise degenerate electric polarization states of the system.

2. Classical $\uparrow\uparrow\downarrow\downarrow$ plateau

In the easy axis anisotropy limit $\gamma \rightarrow 0$ and no magnetoelastic coupling ($\alpha = 0$) our model coincides with the homogeneous frustrated antiferromagnetic Ising chain (ANNNI model). It is known that this model enters the collinear antiphase ($\uparrow\uparrow\downarrow\downarrow$) state at $J_2/J_1 > 0.5$ [51], where J_2 is large enough to make the NNN spin correlations everywhere antiferromagnetic, while NN correlations alternate between values $\pm S^2$. Same as in the quantum case, the analysis of the self-consistent conditions in Eq. 11 shows that the magnetoelastic terms favor alternating distortions, inducing the \mathbb{Z}_2 -symmetric spontaneous polarization.

To explore this classical scenario we performed the self-consistent DMRG computation of the ground state for the same parameters as in the previous subsection, but for a markedly anisotropic easy axis spin-spin interaction, $\gamma = 1/8$. We show in the right panels of Fig. 7 the spin and distortion profiles. They indicate that the spins almost saturate the z component, $\langle S_i^z \rangle \approx \pm 1/2$, following the $\uparrow\uparrow\downarrow\downarrow$ pattern. Spin-spin correlations are close to classical, with $\langle \mathbf{S}_i \cdot \mathbf{S}_{i+1} \rangle \approx 1/4$ for ferromagnetic bonds and $-1/4$ for antiferromagnetic bonds. The distortions do alternate, with short (long) bonds when spin correlations are antiferromagnetic (ferromagnetic). A graphical description of this state is shown in Fig. 9. Same as in the quantum dimerized plateau, alternating distortions lead to a finite spontaneous electric polarization.

It is worth emphasizing the robustness of the spontaneous polarization induced by magnetic instabilities in the pantograph model. We have found the same result in very different regimes, such as the magnetically frustrated $J_1 - J_2$ quantum spin chain, the close to classical frustrated (Ising) chain, and the spin-Peierls chain without magnetic frustration [19]. However, an easy axis

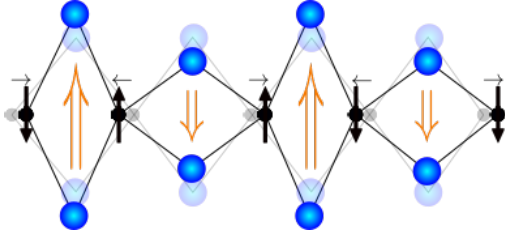


FIG. 9: Schematic picture for the $\uparrow\uparrow\downarrow\downarrow$ plateau state at $M = 0$. The collinear spin configuration represented by black arrows gains magnetic energy by enlarging the exchange coupling of anti-parallel nearest neighbors, shortening their distance. Same as in the quantum dimerized plateau, the influence of these distortions on the dipole strengths (double arrows) produces a ferrielectric configuration with a finite bulk polarization.

anisotropy in the low frustration regime (lower left region in Fig. 1) induces a Néel antiferromagnetic state with homogeneous correlations [74,75] that would eventually destroy the spontaneous polarization.

B. Magnetic excitations

The $M = 0$ configuration remains stable under an external magnetic field h , until it reaches a critical value h_c such that the gain in Zeeman energy of a magnetically excited state is larger than the spin gap. In this situation the system overpasses the $M = 0$ plateau and enters a magnetized regime (see Fig. 5). In order to understand the magnetization process we start by analyzing the features of the $S_{\text{total}}^z = 1$ state; we then check that low magnetization states can be described as a superposition of elementary magnetic excitations.

1. Excitation of the quantum dimerized plateau

There exist extensive studies of the $S_{\text{total}}^z = 1$ excitation of the $S = 1/2$ magnetoelastic spin-Peierls Heisenberg chain, which appears to be fractionalized into two spinons [76]. In the bosonization framework these spinons can be explained as topological solitonic excitations of a sine-Gordon low energy effective continuum theory coupled to the distortion field [77]. Their presence has been checked numerically by different techniques [58] and they are found to condense at the ground state in the presence of a magnetic field.

Relevant to our purpose is the fact that the topological solitons connect different degenerate vacua of the system. In the spin-Peierls Heisenberg chain the ground state is two-fold degenerate and these vacua are the two possibilities of forming singlet pairs along the chain; that is, the two vacua differ by a one-site translation. The sequence of elastic distortions is also shifted by one site across each soliton, as the short bonds belong together

with magnetic singlet pairs. We call each of these vacua a dimerized domain, say A and B. A qualitative picture in Fig. 10 illustrates the two different dimerized domains separated by a soliton.

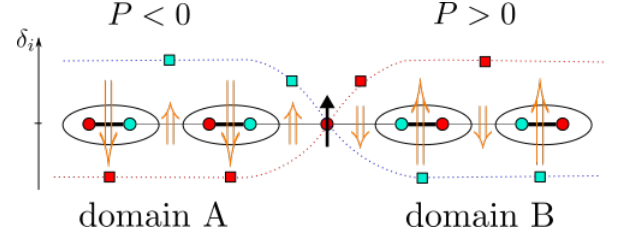


FIG. 10: A magnetic soliton connects the two possible quantum dimer vacua. In this qualitative picture red (cyan) circles represent odd (even) magnetic sites; squares represent the distortions of the bonds at the right of sites with the same color, dotted lines are a guide to follow odd and even site distortions; double arrows represent electric dipoles sitting amidst magnetic sites, in an antiferroelectric configuration. The sequence of spin singlets (ellipses, thick lines indicating enhanced NN exchange) is shifted by one lattice site across the soliton, defining a different dimerized domain. A spin $S = 1/2$ (black arrow) indicates the fractional magnetization carried by the soliton. The sequence of short-long bonds is shifted accordingly. In the presence of the antiferroelectric dipolar background the dimerization defines ferrielectric domains with opposite polarization.

We have checked numerically that solitons also develop in the present model, when distortions are coupled to the amplitudes of antiferroelectrically ordered dipoles. As well, the distortion pattern shows two different domains A and B, separated by the magnetic solitons. *At each domain the dipoles develop a ferrielectric net polarization, pointing in opposite directions.* It is important that both domains are found to have approximately the same length. This is expected from the sine-Gordon low energy theory [78] and numerically observed [79] due to the exponential tails of the soliton profiles, which produce a residual repulsion between them. It has been shown that for higher S_{total}^z the excitations are pairs of solitons distributed as a periodic array, evolving into a sinusoidal magnetization profile [80].

Our numerical results for the $S_{\text{total}}^z = 1$ excitation are shown in Fig. 11. Detailed data shows that the distortions (squares in the upper panel) in odd/even sites are interchanged across the first soliton, as sketched with the same colors in Fig. 10, and interchanged again to its original sequence across the second soliton, so that the short/long bond sequence is shifted by one site at each soliton. The alternation of ferromagnetic/antiferromagnetic correlations (triangles in the lower panel) follows the same sequence as distortions, indicating singlets in two different dimerized domains. The magnetic excitation is localized in the soliton regions, with an incipient $\langle S_i^z \rangle$ spin component. As the soliton regions are wide, in the finite lengths accessible by DMRG $\langle S_i^z \rangle$ does not reach the null value seen in the vacuum

state; instead, distortions and correlations clearly reach their vacuum patterns. Similar behavior has been reported for the excitation of fractional plateau states in the frustrated magnetoelastic spin chain [60,71].

We have also studied higher magnetically excited states, where a pattern of equidistant soliton pairs shows up, thus confirming the described cancellation of electric polarization.

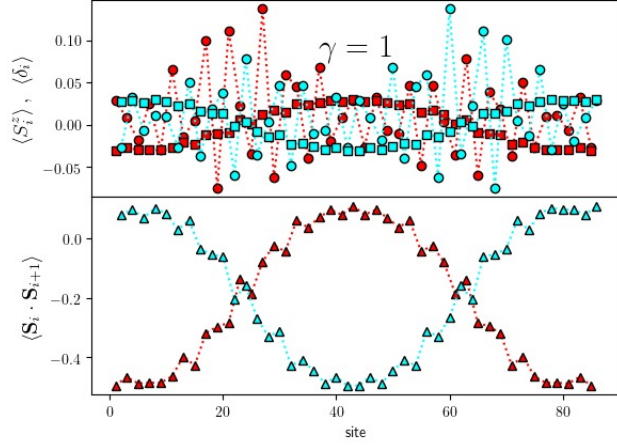


FIG. 11: Local observables in the $S^z_{\text{total}} = 1$ excitation in a chain of 86 sites, in the isotropic case $\gamma = 1$ (with periodic boundary conditions, $J_1 = 0.5$, $J_2 = 0.4$, $J_e = 0.2$, $\alpha = \beta = 0.2$, in the presence of an antiferroelectric dipolar background). Notice that, using periodic boundary conditions, we have changed the chain length to 86 sites for commensurability of the DMRG solution of the $S^z_{\text{total}} = 1$ excitation with the lattice size. Upper panel: local profile of $\langle S^z_i \rangle$ (circles) and distortions δ_i (squares). Lower panel: local spin correlations $\langle \mathbf{S}_i \cdot \mathbf{S}_{i+1} \rangle$ (triangles). The same colors red, cyan in Fig. 10 are used here to visually distinguish odd, even sites and bonds. The magnetic state develops a two-soliton profile for spin correlations, separating equal length domains. The dimerized distortions follow the same profile. The local magnetizations $\langle S^z_i \rangle$ do not vanish, being larger around the soliton regions, but show no clear order. Qualitative features agree with the cartoon in Fig. 10.

2. Excitation of the $\uparrow\uparrow\downarrow$ plateau

Given the Ising-like $\uparrow\uparrow\downarrow$ structure found in the anisotropic case $\gamma = 1/8$ for the $M = 0$ plateau in Fig. 7 (right panels), one could expect that the $S^z_{\text{total}} = 1$ magnetic excitation also looks Ising-like, that is a simple spin flip followed by a rearrangement of classical spins defining sharp domain walls where some second neighbors correlations get frustrated (ferromagnetic).

However, it happens that the system takes advantage of quantum fluctuations to develop solitonic excitations, so that the reduction of $\langle S^z_i \rangle$ in the soliton region lowers

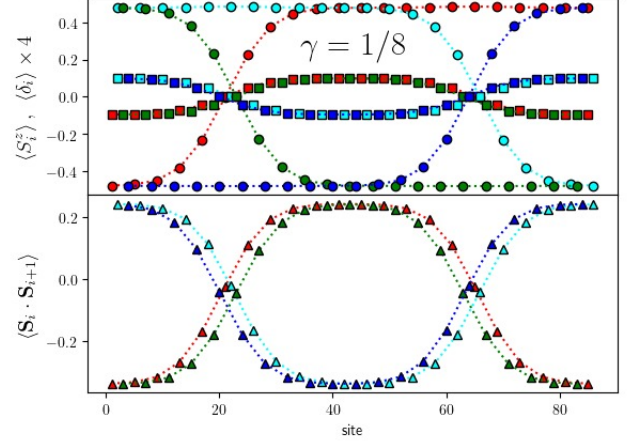


FIG. 12: $S^z_{\text{total}} = 1$ excitation configuration in a chain of 86 sites with periodic boundary conditions ($J_1 = 0.5$, $J_2 = 0.4$, $J_e = 0.2$, $\alpha = \beta = 0.2$, in the presence of an antiferroelectric dipolar background), in the anisotropic case $\gamma = 1/8$. Upper panels: local profile of $\langle S^z_i \rangle$ (circles) and distortions δ_i (squares), in the isotropic case ($\gamma = 1$) and highly anisotropic case ($\gamma = 1/8$). Lower panels: local profile of spin correlations $\langle \mathbf{S}_i \cdot \mathbf{S}_{i+1} \rangle$ (triangles). Four different colors red, cyan, green, blue are used to visually help the location of data every four sites. The system develops two magnetic solitons, separating equal length domains. The $\uparrow\uparrow\downarrow$ spin pattern, as well as the short/long distortion pattern, are shifted by one lattice site across each soliton.

the energy cost of the frustrated second neighbors correlations. Away from the soliton regions, the same as in the quantum case, we find that the alternation of distortions and spin correlations, and the saturated $\uparrow\uparrow\downarrow$ spin pattern, are similar to the classical $S^z_{\text{total}} = 0$ plateau structure but shifted by one lattice site across each soliton. The same as in the isotropic case, *the electric polarization forms ferroelectric domains with the polarization pointing in opposite directions.*

We show in Fig. 12 these results for anisotropy $\gamma = 1/8$ (cf. the $M = 0$ state in Fig. 7, right panels), using a sequence of colors to identify four sublattices. Spins at the left side show a vacuum $\uparrow\uparrow\downarrow$ configuration; spins at odd sites (red and green sublattices) are flipped across the first soliton to connect with a different $\uparrow\uparrow\downarrow$ vacuum; the same happens with spins at even sites (cyan and blue sublattices) across the second soliton. Distortions are dimerized, changing the dimerization domain across each soliton. Spin correlations in the lower panel show that antiparallel spins go along with short bonds in vacuum regions, but quantum fluctuations fade away the expectation value and correlations of spins in the soliton regions. This fact reduces the energy cost of the solitonic “domain wall”, as compared with sharp classical domain walls. As a visual aid, we summarize in Fig. 13 the $\uparrow\uparrow\downarrow$ soliton features in a cartoon picture.

Notice that the solitons in the anisotropic case are

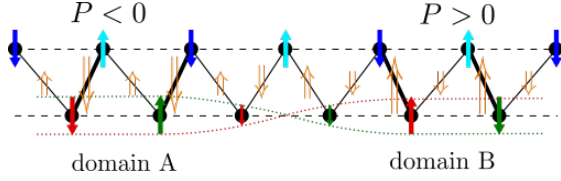


FIG. 13: Schematic description of the first soliton in Fig. 12, connecting two different $\uparrow\uparrow\downarrow\downarrow$ dimerized domains. The linear spin chain can be followed along the rungs of a zig-zag ladder, separating odd sites in the lower leg and even sites in the upper leg. Nearest neighbor exchanges J_1 are represented by solid rung lines and next nearest neighbor exchanges J_2 by dashed straight leg lines. Single arrows represent the $\langle S_i^z \rangle$ component of spins, using the same sublattice colors as in Fig. 12, and orange double arrows represent the electric dipoles between them. Notice that the $\uparrow\uparrow\downarrow\downarrow$ spin order along the chain can be seen as Néel configurations along each leg. The magnetic soliton reverses the spins in the lower leg (indicated as a twist in the dotted lines), leaving unchanged those in the upper leg. The lattice dimerization brings closer the antiparallel nearest neighbor spins, enlarging their exchange couplings (thick solid rungs); thus the magnetic twist produces different dimerization domains with ferroelectric polarizations in opposite directions.

slightly narrower than those in Fig. 11, for the isotropic case $\gamma = 1$. The more anisotropic the interaction, we have checked numerically that the soliton regions gets even narrower. But they do not evolve into sharp domain walls, at least for anisotropies as large as $\gamma = 0.01$ ($\Delta = 100$). It is remarkable that quantum fluctuations play a significant role even in the quasi-classical limit.

The presence of topological solitons, instead of sharp domain walls, is decisive in the formation of equal length $\uparrow\uparrow\downarrow\downarrow$ domains: it is the repulsive residual interaction between solitons what keeps them separated in the finite size chain.

C. Polarization jump driven by magnetic field

At zero electric field, both in the isotropic and the anisotropic cases, the solitonic magnetic excitations separate ferroelectric domains with opposite polarization. This happens not only for $S_{\text{total}}^z = 1$ but for higher excitations described by pairs of solitons. As a consequence, having these domains the same length, the total polarization of the system drops nearly to zero. That is, *the spontaneous electric polarization observed at zero magnetization is switched off by means of the applied magnetic field* [19]. This happens either if the exit from the $M = 0$ plateau is smooth (that is, soliton pairs appear continuously with the magnetic field) or in the case of a metamagnetic jump in which soliton pairs proliferate.

To make apparent the relation between the polarization jump and the onset of magnetization, we plot together in Fig. 14 the polarization and the low magnetization curves in a magnetic field, both for the isotropic

(upper panel) and the anisotropic (lower panel) cases discussed along this work. The spontaneous polarization (red curves, scale in right axis) is computed from the lattice distortions in an antiferroelectric background, according to Eq. 6. In both cases it suddenly drops several orders of magnitude. The magnetization is the same as in Fig. 5, with the addition of an infinite size extrapolation (blue curves, scale in left axis). The infinite size extrapolation of the polarization at the lowest magnetization levels, shown in the insets, clearly proves that the polarization switch off is a bulk magnetoelectric effect occurring at the onset of magnetization. Beyond the ex-

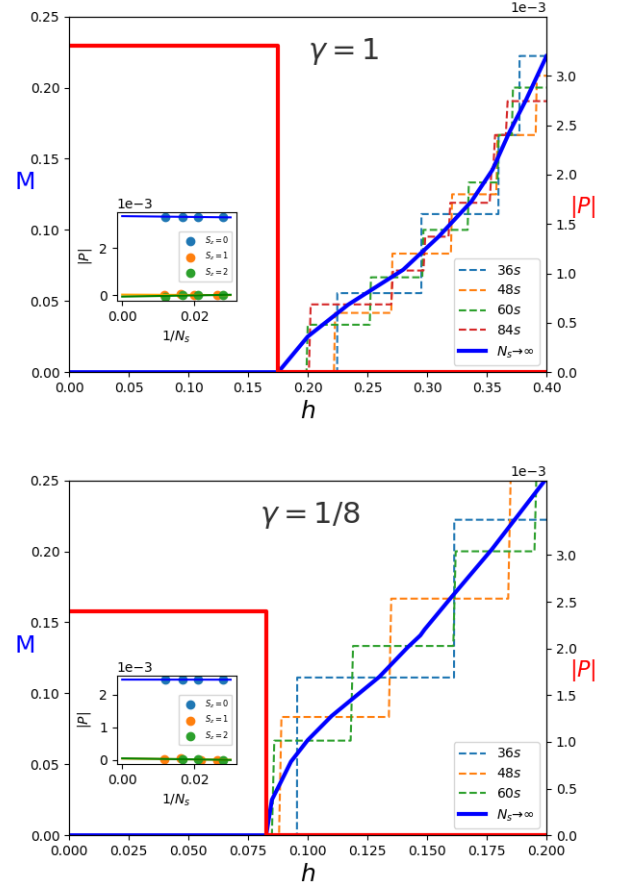


FIG. 14: Polarization curves (red solid lines, scale in the right axis in units of p_0) in an external magnetic field for the isotropic $\gamma = 1$ and the anisotropic $\gamma = 1/8$ models ($J_1 = 0.5$, $J_2 = 0.4$, $J_e = 0.2$, $\alpha = \beta = 0.2$), in the presence of an antiferroelectric dipolar background). Magnetization curves in the low M region (extrapolated as blue solid lines, scale in the left axis) are also plotted for comparison. In both cases the system supports a finite spontaneous polarization at low magnetic fields, while $S_{\text{total}}^z = 0$, but a sudden drop is observed once the system exits the $M = 0$ magnetic plateau. The polarization curves follow from finite size results and infinite size extrapolation. Insets: finite size scaling for the polarizations obtained for $S_{\text{total}}^z = 0, 1, 2$ shows almost no size dependence.

cited $S_{\text{total}}^z = 1$ and $S_{\text{total}}^z = 2$ states, with polarization

shown in the insets, we have checked that the further increase of the magnetization introduces extra pairs of solitons. These appear uniformly spread along the chain, as it also occurs in the magnetoelastic case [80], separating different dimerization domains and producing the drop of the electric polarization observed in Fig. 14 for arbitrary non vanishing magnetization.

Such magnetically driven polarization jumps are a source of intrigue in many multiferroic materials. For instance, $\text{Lu}_2\text{MnCoO}_6$ [16] and $\text{Er}_2\text{CoMnO}_6$ [17] show a polarization jump when exiting the observed $M = 0$ magnetization plateau. Closely related are the polarization jumps observed in $\text{R}_2\text{V}_2\text{O}_7$ ($\text{R} = \text{Ni}, \text{Co}$) when entering and exiting the $M = 1/2$ magnetization plateau [81]. We expect that the present results could help in fitting actual parameters in these materials and explain the observed jumps.

D. Polarization flip controlled by very low electric fields

Measures of spontaneous polarization are usually made with the help of a tiny poling field, to lift the degeneracy between the possible spontaneous orientations. Once done, a coercive field much larger than the poling one is required to flip the bulk polarization.

In the present model it is also interesting to discuss the effect of a poling electric field when the polarization has been switched off by a magnetic field larger than the critical one, strong enough to magnetize and depolarize the system by the creation of pairs of different ferrielectric domains. It happens that the domains with polarization pointing along the poling field are energetically favored, hence pushing apart the soliton walls at their ends to lower the total system energy. As the displacement of solitonic domain boundaries in large systems has very small energy cost, a high electric susceptibility is expected in this regime. In consequence, the polarization cancellation is not perfect and the system exhibits a small net polarization in the direction of the electric field. From this situation, as soon as the magnetic field is turned off, it is expected that the orientation of the much larger recovered spontaneous polarization follows the preferred orientation set by the poling field in the magnetized regime.

One can think of designing a multiferroic memory storage in which information, in the form of a polarized spot, is controlled by a low electric field signal with the help of a brief but strong magnetic blast: a magnetic field, carrying no information, would erase the previously "written" polarization, which is then "rewritten" in the desired (up or down) orientation by the simultaneous presence of a poling low electric field (low voltage bias). The procedure is sketched in Fig. 15. Such a device would show a giant electric response, and could be the basis for an efficient memory writing/reading device.

In order to support these considerations we show in

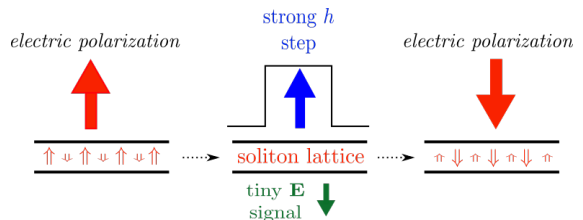


FIG. 15: A magnetic field step, in any orientation and strong enough to magnetize the system, produces electric depolarization. In combination with a tiny poling field signal, it can be used to reverse the spontaneous polarization \mathbf{P} . This could be the basis for storing information in a dipolar memory bit.

Fig. 16 how the equal length domains already seen in Figs. 11 and 12 (shaded symbols here) are modified in the presence of a small electric field $\epsilon = 0.01$: the central domain, with polarization along the field, indeed gets wider. We note that in the computationally accessible finite size chains the effect is more pronounced in the anisotropic case, where the solitons are narrower and their residual repulsion is less manifest.

V. SUMMARY AND PERSPECTIVES

In the present work we have extended and improved a microscopic mechanism of magnetoelectric coupling mediated by lattice distortions, previously introduced by the authors in [19], into a realistic model for type II collinear multiferroic materials. Essential ingredients to match with experimental observations are the easy axis anisotropy $\Delta > 1$ (expressed for convenience as $\gamma < 1$) favoring collinearity, the magnetic frustration J_2/J_1 leading to the "uudd" spin ground state and the Coulomb-like long range dipole-dipole interaction establishing the antiferroelectric order, all of these in the absence of external fields. Motivated by the variety of known multiferroic materials, which includes the $SU(2)$ symmetric as well as strongly easy axis anisotropic spin interactions, we have explored the proposed model from the Heisenberg isotropic regime $\Delta = 1$ up to Ising-like anisotropic cases $\Delta \gg 1$.

The microscopic mechanism may be described by a spin-dipole-Peierls Hamiltonian, where the indirect magnetoelectric coupling arises from a combination of a spin-Peierls like magnetoelectric coupling, which is known to lead to an elastic dimerization instability, and a pantograph mechanism that relates the strength of electric dipolar moments to lattice deformations. Both mechanisms are ubiquitous in multiferroic materials, specially when competing magnetic interactions frustrate an antiferromagnetic Néel configuration. Magnetic and electric degrees of freedom can thus either cooperate or compete in provoking lattice instabilities, in a precise way expressed in the selfconsistent key Eqs. 11.

We have argued theoretically and proven numerically, by extensive DMRG computations, that in a wide param-

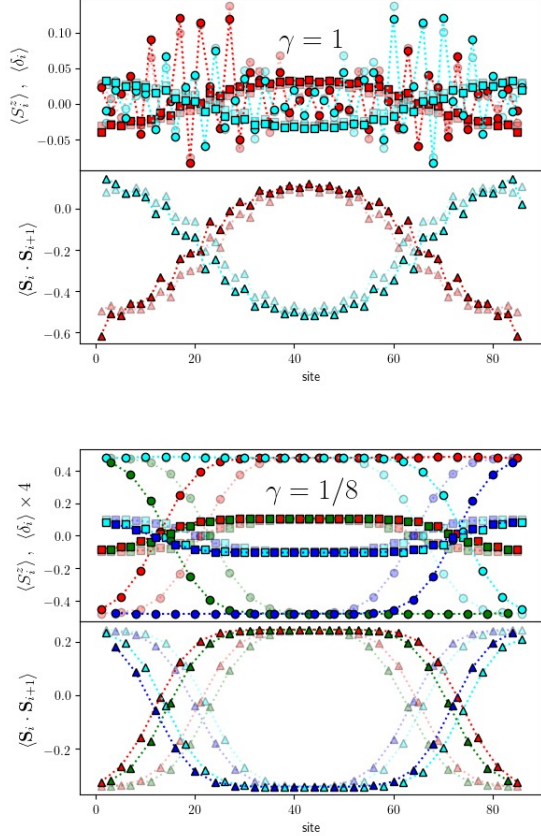


FIG. 16: A small electric field provokes the displacement of the solitons in the $S_z = 1$ configuration, enlarging the domain with electric polarization along the field. The solid symbols correspond to an electric field $\epsilon = 0.01$, with the rest of the parameters as in Figs. 11, 12 (repeated here in shaded symbols for comparison). The same effect is observed both in the isotropic and the anisotropic case.

eter region, starting at the isotropic $SU(2)$ Heisenberg model and going up to an extreme anisotropic ANNNI model, the system has a gapped magnetic ground state associated to dimerized lattice distortions. Main consequences are the zero magnetization plateaus in the magnetization curves and the emergence of an spontaneous ferrielectric bulk polarization (an antiferroelectric with a remanent polarization), with two possible degenerate orientations (\mathbb{Z}_2 symmetry).

In the presence of an external magnetic field exceeding a critical value, related to the spin gap, low magnetization excitations develop as pairs of topological solitons that separate different dimerized domains carrying opposite ferrielectric polarizations. A lattice of equidistant solitons grows along the system, producing a sharp switch off in the bulk polarization. This mechanism, robust due to its topological character, could be at the root of the bulk polarization jumps observed in many different multiferroic materials. We expect that the present paradigm

might be fitted to actual experimental parameters and be identified as one of the microscopic mechanisms behind magnetically induced polarization jumps.

We have also found a novel polarization state at intermediate electric fields with $\uparrow\uparrow\downarrow$ periodicity, exclusively due to the long range character of the dipolar interactions frustrating the antiferroelectric order. Such a period three dipolar configuration, combined with the $M = 1/3$ magnetic plateau state found at intermediate magnetic fields, could give rise to interesting magnetoelectric cross effects. This will be studied elsewhere.

Regarding technological interest, a material described by our model is classified as a *ferrielectric*. It has a spontaneous \mathbb{Z}_2 polarization due to dipolar imbalance that can be easily controlled by applied fields. In fact the presence of a small poling electric field gives rise to a relative displacement of the solitonic domain walls, making the polarization of the magnetized states not to be completely turned off. Then a demagnetization would select a preferred orientation for the spontaneous polarization. This property could be used, for instance, to engineer polarized memory storage devices controllable by very low electric signals. From a different point of view, the present work could guide the design and manufacture of composite artificial multiferroic systems, such as multilayers (see for instance [82]) where the mechanical strain transfer couples ferroelectricity and ferromagnetism, or even regularly nano-patterned arrays (see for instance [83]) where flexoelectricity couples magnetostriuctive strain gradients with electric polarization, in different materials. The technological control of multiferroicity in these multiphase composite systems is rapidly progressing and could in a future be the alternative to chemically synthesized multiferroic compounds. We hope that the understanding of the mechanisms of multiferroicity at the atomic scale will shed light on the effective magnetoelectric coupling mechanisms taking place at the nanometer scale.

The pantograph mechanism, which is the key ingredient in our proposal to generate the magnetoelectric coupling, encodes the relation between the dipolar moments and their lattice environment and is present as well in two or three dimensional systems. Appropriate extensions of the present model can be written taking into account detailed crystallographic data. In these higher dimensional settings the isolated solitons could become extended walls; the predicted magnetically driven polarization switch off will probably survive to these generalizations.

Acknowledgements

The authors are grateful to A.E. Trumper for early interest and comments on this work. D.C.C. acknowledges useful discussions with S.-W. Cheong, D.I. Khomskii and C.D. Batista. This work was partially supported by CONICET (Grants No. PIP 2015-813 and No. PIP

2015-364), Argentina.

- ¹ S.-W. Cheong, M. Mostovoy, *Nature Mater.* **6**, 13 (2007).
- ² J. van den Brink, D.I. Khomskii, *J. Phys.: Condens. Matter* **20**, 434217 (2008).
- ³ P.G. Radaelli and L.C. Chapon, *J. Phys.: Condens. Matter* **20**, 434213 (2008).
- ⁴ S. Dong, H. Xiang, and E. Dagotto, *Natl. Sci. Rev.* **6**, 629 (2019).
- ⁵ M.L. Medarde, *J. Phys.: Condens. Matter* **9**, 1679 (1997).
- ⁶ Y.J. Choi, H.-T. Yi, S. Lee, Q. Huang, V. Kiryukhin, and S.-W. Cheong, *Phys. Rev. Lett.* **100**, 047601 (2008); R. Flint, H.-T. Yi, P. Chandra, S.-W. Cheong and V. Kiryukhin, *Phys. Rev. B* **81**, 092402 (2010); M. Nishida, F. Ishii, and M. Saito, *J. Phys. Soc. Jpn.* **83**, 124711 (2014); V.S. Zapf, B.G. Ueland, M. Laver, M. Lonsky, M. Pohlitz, J. Müller, T. Lancaster, J.S. Möller, S.J. Blundell, J. Singleton, J. Mira, S. Yáñez-Vilar, and M.A. Señarís-Rodríguez, arXiv:1409.5072 (2014).
- ⁷ F. Damay, C. Martin, V. Hardy, G. André, S. Petit, and A. Maignan, *Phys. Rev. B* **83**, 184413 (2011).
- ⁸ S.V. Streltsov, A.I. Poteryaev, and A.N. Rubtsov, *J. Phys.: Condens. Matter* **27**, 165601 (2015).
- ⁹ I.A. Sergienko, C. Şen and E. Dagotto, *Phys. Rev. Lett.* **97**, 227204 (2006).
- ¹⁰ S. Dong, R. Yu, S. Yunoki, J.-M. Liu, and E. Dagotto, *Eur. Phys. J. B* **71**, 339 (2009).
- ¹¹ Y. Tokunaga, N. Furukawa, H. Sakai, Y. Taguchi, T. Arima, and Y. Tokura, *Nature Mater.* **8**, 558 (2009).
- ¹² G. Giovannetti, A. Stroppa, S. Picozzi, D. Baldomir, V. Pardo, S. Blanco-Canosa, F. Rivadulla, S. Jodlauk, D. Niermann, J. Rohrkamp, T. Lorenz, S. Streltsov, D.I. Khomskii, and J. Hemberger, *Phys. Rev. B* **83**, 060402(R) (2011).
- ¹³ S. Catalano, M. Gibert, J. Fowlie, J. Íñiguez, J.-M. Triscone, and J. Kreisel, *Rep. Prog. Phys.* **81** (2018) 046501.
- ¹⁴ J. Blasco, J.L. García-Muñoz, J. García, G. Subías, J. Stankiewicz, J.A. Rodríguez-Velamazán, and C. Ritter, *Phys. Rev. B* **96**, 024409 (2017).
- ¹⁵ S. Yáñez-Vilar, E.D. Mun, V.S. Zapf, B.G. Ueland, J.S. Gardner, J.D. Thompson, J. Singleton, M. Sánchez-Andújar, J. Mira, N. Biskup, M.A. Señarís-Rodríguez, and C.D. Batista, *Phys. Rev. B* **84**, 134427 (2011).
- ¹⁶ S. Chikara, J. Singleton, J. Bowlan, D.A. Yarotski, N. Lee, H.Y. Choi, Y.J. Choi, and V.S. Zapf, *Phys. Rev. B* **93**, 180405(R) (2016).
- ¹⁷ M.K. Kim, J.Y. Moon, S.H. Oh, D.G. Oh, Y.J. Choi, and N. Lee, *Scientific Reports* **9**, 5456 (2019).
- ¹⁸ H.Y. Zhou, H.J. Zhao, W.Q. Zhang, and X.M. Chen, *Appl. Phys. Lett.* **106**, 152901 (2015).
- ¹⁹ D.C. Cabra, A.O. Dobry, C.J. Gazza, and G.L. Rossini, *Phys. Rev.* **100**, 161111(R) (2019).
- ²⁰ Y.S. Hou, J.H. Yang, X.G. Gong, and H.J. Xiang, *Phys. Rev. B* **88**, 060406 (2013).
- ²¹ K. Shimamoto, S. Mukherjee, S. Manz, J.S. White, M. Trassin, M. Kenzelmann, L. Chapon, T. Lippert, M. Fiebig, C.W. Schneider, and Christof Niedermayer, *Scientific Reports* **7**, 44753 (2017).
- ²² S.T. Bramwell and M.J.P. Gingras, *Science* **294**, 1495 (2001).
- ²³ M.J.P. Gingras and P.A. McClarty, *Rep. Prog. Phys.* **77** 056501 (2014).
- ²⁴ J.G. Rau and M.J.P. Gingras, *Annu. Rev. Condens. Matter Phys.* **10**, 357 (2019).
- ²⁵ D. Slobinsky, L. Pili, G. Baglietto, S.A. Grigera, and R.A. Borzi, arXiv:2011.15017.
- ²⁶ Y. Shi, Y. Guo, X. Wang, A.J. Princep, D. Khalyavin, P. Manuel, Y. Michiue, A. Sato, K. Tsuda, S. Yu, M. Arai, Y. Shirako, M. Akaogi, N. Wang, K. Yamaura, and A.T. Boothroyd, *Nature Mater.* **12**, 1024 (2013); H.M. Liu, Y.P. Du, Y.L. Xie, J.-M. Liu, C.-G. Duan, and X. Wan, *Phys. Rev. B* **91**, 064104 (2015); F. Jin, L. Wang, A. Zhang, J. Ji, Y. Shi, X. Wang, R. Yu, J. Zhang, E.W. Plummer, and Q. Zhang, *PNAS* **116**, 20322 (2019).
- ²⁷ F. Devonshire, *Adv. Phys.* **3**, 85 (1954).
- ²⁸ B. J. Gibson, R. K. Kremer, A. V. Prokofiev, W. Assmus, and G. J. McIntyre, *Physica B* **350**, E253 (2004).
- ²⁹ Y. Yasui, Y. Naito, K. Sato, T. Moyoshi, M. Sato, and K. Kakurai, *J. Phys. Soc. Jpn.* **77**, 023712 (2008).
- ³⁰ S. Park, Y. J. Choi, C. L. Zhang, and S.-W. Cheong, *Phys. Rev. Lett.* **98**, 057601 (2007).
- ³¹ S. Seki, Y. Yamasaki, M. Soda, M. Matsuura, K. Hirota, and Y. Tokura, *Phys. Rev. Lett.* **100**, 127201 (2008).
- ³² Y. Yasui, K. Sato, Y. Kobayashi, and M. Sato, *J. Phys. Soc. Jpn.* **78**, 084720 (2009).
- ³³ S. Seki, T. Kurumaji, S. Ishiwata, H. Matsui, H. Murakawa, Y. Tokunaga, Y. Kaneko, T. Hasegawa, and Y. Tokura, *Phys. Rev. B* **82**, 064424 (2010).
- ³⁴ L. Zhao, T.-L. Hung, C.-C. Li, Y.-Y. Chen, M.-K. Wu, R. K. Kremer, M. G. Banks, A. Simon, M.-H. Whangbo, C. Lee, J. S. Kim, I. Kim, and K.H. Kim, *Adv. Mater.* **24**, 2469 (2012).
- ³⁵ B. Willenberg, M. Schäpers, K. C. Rule, S. Süllo, M. Reehuis, H. Ryll, B. Klemke, K. Kiefer, W. Schottenhamel, B. Büchner, B. Ouladdiaf, M. Uhlarz, R. Beyer, J. Wosnitza, and A. U. B. Wolter, *Phys. Rev. Lett.* **108**, 117202 (2012).
- ³⁶ Y. Yasui, M. Sato, and I. Terasaki, *J. Phys. Soc. Jpn.* **80**, 033707 (2011); Y. Yasui, Y. Yanagisawa, M. Sato, and I. Terasaki, *J. Phys.: Conf. Ser.* **320**, 012087 (2011).
- ³⁷ J. M. Law, P. Reuvekamp, R. Glaum, C. Lee, J. Kang, M.-H. Whangbo, and R. K. Kremer, *Phys. Rev. B* **84**, 014426 (2011).
- ³⁸ B. Koteswararao, K. Yoo, F.C. Cho, and K.H. Kim, *APL Materials* **4**, 036101 (2016).
- ³⁹ T. Giamarchi, *Quantum Physics in One Dimension*, (Oxford University Press, 2004).
- ⁴⁰ See for instance A. Auerbach, *Interacting electrons and quantum magnetism*, (Springer-Verlag, Heidelberg, 1994).
- ⁴¹ F. Seno and J. M. Yeomans, *Phys. Rev. B* **50**, 10385 (1994).
- ⁴² F.J. Dyson, *Phys. Rev.* **102**, 1217 (1956); S.V. Maleev, *Sov. Phys. JETP* **6**, 776 (1958).
- ⁴³ F. Blanco, Msc. Thesis, Universidad Nacional de La Plata, Argentina (unpublished).
- ⁴⁴ F.D.M. Haldane, *Phys. Rev. B* **25**, 4925 (1982).
- ⁴⁵ K. Okamoto and K. Nomura, *Phys. Lett. A* **169**, 433 (1992).

- ⁴⁶ S. Eggert, Phys. Rev. B **54**, R9612(R) (1996).
- ⁴⁷ C.K. Majumdar and D. Ghosh, J. Math. Phys. **10**, 1388 (1969).
- ⁴⁸ S.R. White and I. Affleck, Phys. Rev. B **54**, 9862 (1996).
- ⁴⁹ D. Allen and D. Senechal, Phys. Rev. B **55**, 299 (1997).
- ⁵⁰ A.A. Nersisyan, A.O. Gogolin, and F.H.L. Essler, Phys. Rev. Lett. **81**, 910 (1998).
- ⁵¹ W. Selke, Phys. Rep. **170**, 213 (1988).
- ⁵² R. Resta, Europhys. Lett. **22**, 133 (1993).
- ⁵³ G. Radtke, A. Saúl, H. A. Dabkowska, M. B. Salamon, and M. Jaime, Proc. Natl. Acad. Sci. USA **112**, 1971 (2015).
- ⁵⁴ X. Yao and V.C. Lo, Journal of Applied Physics **104**, 083919 (2008).
- ⁵⁵ N. Spalding, in *Physics of Ferroelectrics: a Modern Perspective*, edited by K. Rabe, Ch.H. Ahn and J.-M. Triscone (Springer-Verlag, Heidelberg, 2007).
- ⁵⁶ M. Naka and S. Ishihara, Sci. Rep **6**, 20781 (2016).
- ⁵⁷ K. A. Müller and H. Burkard, Phys. Rev. B **19**, 3593 (1979); P. Chandra, G.G. Lonzarich, S.E. Rowley, and J.F. Scott, Rep. Prog. Phys. **80** 112502 (2017); C. Enderlein, J. Ferreira de Oliveira, D A. Tompsett, E. Baggio Saitovitch, S.S. Saxena, G.G. Lonzarich, and S.E. Rowley, Nat. Commun. **11**, 4852 (2020).
- ⁵⁸ A.E. Feiguin, J.A. Riera, A.O. Dobry, and H.A. Ceccatto, Phys. Rev. B **56**, 14607 (1997).
- ⁵⁹ S.R. White, Phys. Rev. Lett. **69**, 2863 (1992).
- ⁶⁰ C.J. Gazza, A.O. Dobry, D.C. Cabra, and T. Vekua, Phys. Rev. B **75**, 165104 (2007).
- ⁶¹ M.C. Cross and D.S. Fisher, Phys Rev B **19**, 402 (1979).
- ⁶² J.W. Bray, L.V. Interrante, I.S. Jacobs, and J.C. Bonner, in *Extended Linear Chain Compounds*, edited by J.C. Miller (Plenum, New York, 1982).
- ⁶³ F. Becca and F. Mila, Phys. Rev. Lett. **89**, 037204 (2002).
- ⁶⁴ J. Sirker, A. Klümper, and K. Hamacher, Phys. Rev. B **65**, 134409 (2002).
- ⁶⁵ K. Penc, N. Shannon, and H. Shiba, Phys. Rev. Lett. **93**, 197203 (2004).
- ⁶⁶ C.H. Aits, U. Löw, A. Klümper, and W. Weber, Phys. Rev. B **74**, 014425 (2006).
- ⁶⁷ S. Bissola, V. Lante, A. Parola, and F. Becca Phys. Rev. B **75**, 184444 (2007).
- ⁶⁸ D. C. Cabra, M. Moliner, and F. Stauffer, Phys. Rev. B **74**, 014428 (2006).
- ⁶⁹ T. Vekua, D.C. Cabra, A.O. Dobry, C.J. Gazza, and D. Poilblanc, Phys. Rev. Lett. **96**, 117205 (2006).
- ⁷⁰ K. Okunishi and T. Tonegawa, Journal of the Physical Society of Japan **3**, 479 (2003).
- ⁷¹ K. Hida and I. Affleck, J. Phys. Soc. Japan **74**, 1849 (2005).
- ⁷² T. Kimura, T. Goto, H. Shintani, K. Ishizaka, T. Arima, and Y. Tokura, Nature **426**, 55 (2003).
- ⁷³ N. Hur, S. Park, P.A. Sharma, J.S. Ahn, S. Guha, and S-W. Cheong, Nature **429**, 392 (2004).
- ⁷⁴ S. Inagaki and H. Fukuyama, J. Phys. Soc. Jpn. **52**, 2504 (1983).
- ⁷⁵ P. Li and Y. Chen, Physics Letters A **374**, 453 (2010).
- ⁷⁶ M. Arai, M. Fujita, M. Motokawa, J. Akimitsu, and S.M. Bennington, Phys. Rev. Lett. **77**, 3649 (1996).
- ⁷⁷ T. Nakano and H. Fukuyama, J. Phys. Soc. Jpn. **49**, 1679 (1980).
- ⁷⁸ N. Manton and P. Sutcliffe, *Topological solitons* (Cambridge University Press, Cambridge, 2004).
- ⁷⁹ D. Mastrogiuseppe, C. Gazza, and A. Dobry, J. Phys.: Condens. Matter **20**, 135223 (2008).
- ⁸⁰ T. Lorenz, B. Büchner, P.H.M. van Loosdrecht, F. Schönfeld, G. Chouteau, A. Revcolevschi and G. Dhalenne, Phys. Rev. Lett. **81**, 148 (1998).
- ⁸¹ R. Chen, J. F. Wang, Z. W. Ouyang, Z. Z. He, S. M. Wang, L. Lin, J. M. Liu, C. L. Lu, Y. Liu, C. Dong, C. B. Liu, Z. C. Xia, A. Matsuo, Y. Kohama, and K. Kindo, Phys. Rev. B **98**, 184404 (2018).
- ⁸² T. Taniyama, J. Phys.: Condens. Matter **27**, 504001 (2015).
- ⁸³ S. Poddar, P. de Sa, R. Cai, L. Delannay, B. Nysten, L. Piraux, and A.M. Jonas, ACS Nano **12**, 576 (2018),